Permporosimetry performed following the techniques of (*17*) indicated that the trimer-TPA–grown films are free of cracks and pinholes detectable by this technique. FCOM performed after impregnation with fluorescein (*23*) revealed only a small number of grain boundary defects. These findings for the trimer-TPA–grown films are in sharp contrast with the corresponding ones for the c-oriented films, which showed the presence of a large density of grain boundary defects, and for the [h0h]-oriented films, which showed the presence of microcracks formed during calcination. We previously attributed the poor xylene separation performance of the c-oriented films to the presence of the grain boundary defects detectable by FCOM (*23*). We also found that to obtain high separation factors from [h0h]-oriented films, a crack reparation post treatment should be used (*23*) but that this led to considerable variation in flux and separation factors (*23*). This variation is seen by the scattered permeation data associated with area (4) in Fig. 4E. The improved reproducibility in the separation performance of the trimer-TPA–grown films is reflected by the smaller spread associated with area (7) in Fig. 4E.

Improved functionality ZSM-5 membranes, as demonstrated by high-flux, high-selectivity xylene isomer separation, can be achieved by appropriate channel orientation throughout a thin film. The films were synthesized by seeded growth of oriented particle monolayers and use of SDAs that, in addition to directing the formation of the zeolite structure, act as crystal growth rate modifiers to achieve the appropriate balance between in-plane and out-of-plane growth. The implementation of crystal shape engineering by the use of SDA polycations as shape or habit modifiers should be applicable for the fabrication of other improved zeolite and molecular sieve films.

**References and Notes**
1. M. E. Davis, *Nature* **417**, 813 (2002).
2. T. Bein, *Chem. Mater.* **8**, 1636 (1996).
3. M. Tsapatsis *et al.*, *CATTECH* **3**, 148 (2000).
4. J. Caro, M. Noack, P. Kolsch, R. Schafer, *Micropor. Mesopor. Mater.* **38**, 3 (2000).
5. G. A. Ozin, A. Kuperman, A. Stein, *Angew. Chem. Int. Ed. Engl.* **28**, 359 (1989).
6. C. J. Gump, V. A. Tuan, R. D. Noble, J. L. Falconer, *Ind. Eng. Chem. Res.* **40**, 565 (2001).
7. Z. Wang, Y. Yan, *Chem. Mater.* **13**, 1101 (2001).
8. S. Mintova, V. Valtchev, V. Engstrom, B. J. Schoeman, J. Sterte, *Micropor. Mater.* **11 (3-4)**, 149 (1997).
9. M. Kondo, M. Komori, H. Kita, K. Okamoto, *J. Membr. Sci.* **133**, 133 (1997).
10. J. Dong, Y. S. Lin, M. Z. C. Hu, R. A. Peascoe, E. A. Payzant, *Micropor. Mesopor. Mater.* **34**, 241 (2000).
11. Z. Wang, H. Wang, A. Mitra, L. Huang, Y. Yan, *Adv. Mater.* **13**, 746 (2001).
12. T. C. Merkel *et al.*, *Science* **296**, 519 (2002).
13. J. W. Koros, R. Mahajan, *J. Membr. Sci.* **175**, 181 (2000).
14. M. B. Shiflett, H. C. Foley, *Science* **285**, 1902 (1999).
15. R. M. de Vos, H. Verweij, *Science* **279**, 1710 (1998).
16. Y. Lu *et al.*, *Nature* **389**, 364 (1997).
17. J. Hedlund *et al.*, *Micropor. Mesopor. Mater.* **52**, 179 (2002).
18. L. T. Y. Au, W. Y. Mui, P. S. Lau, C. T. Ariso, K. L. Yeung, *Micropor. Mesopor. Mater.* **47**, 203 (2001).
19. A. Gouzinis, M. Tsapatsis, *Chem. Mater.* **10**, 2497 (1998).
20. M. Noack *et al.*, *Micropor. Mesopor. Mater.* **49**, 25 (2001).
21. Y. Yan, M. E. Davis, G. R. Gavalas, *J. Membr. Sci.* **123**, 95 (1997).
22. M. Nomura, T. Yamaguchi, S. Nakao, *Ind. Eng. Chem. Res.* **36**, 4217 (1997).
23. G. Xomeritakis, Z. Lai, M. Tsapatsis, *Ind. Eng. Chem. Res.* **40**, 544 (2001).
24. E. M. Flanigen *et al.*, *Nature* **271**, 512 (1978).
25. W. M. Meier, D. H. Olson, Ch. Baerlocher, *Atlas of Zeolite Framework Types* (Elsevier, London, 1996).
26. B. M. Lok, T. R. Cannan, C. A. Messina, *Zeolites* **3**, 282 (1983).
27. S. L. Burkett, M. E. Davis, *J. Phys. Chem.* **98**, 4647 (1994).
28. G. H. Kuhl, C. Hill, U.S. Patent 4,585,638 (1986).
29. E. de Vos Burchart, J. C. Jansen, B. van de Graaf, H. van Bekkum, *Zeolites* **13**, 216 (1993).
30. L. W. Beck, M. E. Davis, *Micropor. Mesopor. Mater.* **22**, 107 (1998).
31. B. J. Schoeman, J. Sterte, J. E. Otterstedt, *J. Chem. Soc. Chem. Commun.* **12**, 994 (1993).
32. M. C. Lovallo, M. Tsapatsis, *AIChE J.* **42**, 3020 (1996).
33. L. C. Boudreau, M. Tsapatsis, *Chem. Mater.* **9**, 1705 (1997).
34. K. Ha, Y. J. Lee, H. J. Lee, K. B. Yoon, *Adv. Mater.* **12**, 1114 (2000).
35. L. J. Song, Z. L. Sun, L. V. C. Rees, *Micropor. Mesopor. Mater.* **55**, 31 (2002).
36. K. Keizer, A. J. Burggraaf, Z. A. E. P. Vroon, H. Verweij, *J. Membr. Sci.* **147**, 159 (1998).

# REPORTS

## On the Origins of Morphological Complexity in Block Copolymer Surfactants

**Sumeet Jain and Frank S. Bates***

Amphiphilic compounds such as lipids and surfactants are fundamental building blocks of soft matter. We describe experiments with poly(*1,2*-butadiene-*b*-ethylene oxide) (PB-PEO) diblock copolymers, which form Y-junctions and three-dimensional networks in water at weight fractions of PEO intermediate to those associated with vesicle and wormlike micelle morphologies. Fragmentation of the network produces a nonergodic array of complex reticulated particles that have been imaged by cryogenic transmission electron microscopy. Data obtained with two sets of PB-PEO compounds indicate that this type of self-assembly appears above a critical molecular weight. These block copolymers represent versatile amphiphiles, mimicking certain low molecular weight three-component (surfactant/water/oil) microemulsions, without addition of a separate hydrophobe.

The manipulation of interfacial curvature and topology plays a central role in the creation of soft materials (*1*). Living cells, mayonnaise, and fracturing fluids used in oil recovery are representative examples of heterogeneous systems containing coexisting hydrophilic and hydrophobic domains assembled in precise ways through the action of ubiquitous amphiphilic compounds such as lipids, soaps, and other surfactants (*2*). Macromolecular surfactants, such as poly(butadiene-*b*-ethylene oxide) (PB-PEO) diblock copolymers, offer important materials advantages not associated with conventional low molecular weight amphiphiles (*3*). For example, vesicles and wormlike micelles can be chemically cross-linked without structural disruption, leading to dramatic modifications of static and dynamic mechanical properties (*4*, *5*). Over the past decade, Eisenberg and co-workers (*6–8*) have demonstrated that block copolymers also afford access to a cornucopia of complex morphological assemblies through clever processing strategies.

For several years we have explored various similarities and differences in the thermodynamic and processing properties of conventional and polymeric amphiphiles (*4*, *9–11*). Here, we document a surprising

Department of Chemical Engineering and Materials Science, University of Minnesota, Minneapolis, MN 55455, USA.

*To whom correspondence should be addressed. E-mail: bates@cems.umn.edu

result: network formation in two-component dilute aqueous solutions of PB-PEO. Previous experiments with relatively low molecular weight macromolecular surfactants produced three basic structural elements: spheres (S), cylinders (C), and bilayers (B). These zero-, one-, and two-dimensional structures are readily dispersed in water at low concentration as spherical micelles, wormlike micelles, and vesicles, respectively, mimicking the well-established states of aggregation created when low molecular weight amphiphiles are mixed with water (*12*). Here we demonstrate the formation of "Y-junctions," which assemble into a dense, three-dimensional network (N) accompanied by macroscopic phase separation. Isolated fragments of the network have been evaluated with cryogenic transmission electron microscopy (cryo-TEM), from which we deduce that the Y-junction is preferred thermodynamically above a critical surfactant molecular weight at compositions between those associated with the B and C morphologies. These findings are consistent with theoretical predictions recently developed (*13*, *14*) and demonstrated (*15*, *16*) with traditional three-component (surfactant/oil/water) microemulsions, signaling a fundamental transition in self-assembly behavior as the amphiphile molecular weight is increased beyond a critical value.

Two sets of PB-PEO diblock copolymers (Scheme 1), each containing constant molecular weight poly(*1,2*-butadiene) blocks ($M_{n,PB}$ = 2500 and 9200 g/mol) and varying weight fractions of PEO ($w_{PEO}$), were synthesized with anionic polymerization techniques described elsewhere (*17*). Fifteen compounds with degree of polymerization $N_{PB}$ = 46 and $0.30 \leq w_{PEO} \leq 0.64$, and 13 with $N_{PB}$ = 170 and $0.24 \leq w_{PEO} \leq 0.62$, were prepared; in all cases, the compounds had relatively narrow molecular weight distribution, $M_w/M_n < 1.1$. These diblock copolymers were mixed with measured amounts of distilled water, generally at a concentration of 1 weight percent (wt%), and stirred at room temperature.

Solution morphologies were characterized with cryo-TEM, a powerful microscopy technique capable of imaging molecular-scale structures in thin (~100 to 300 nm) films of vitrified aqueous solutions. The results for the 1% mixtures are summarized in Fig. 1. With $N_{PB}$ = 46, we find the classic sequence of dispersed structures
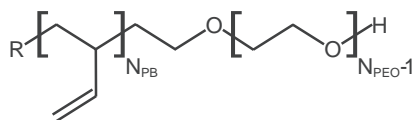
(B, C, and S) separated by mixed morphology regimes (B + C and C + S) with increasing PEO content, in agreement with an earlier report (*11*). Increasing the size of the hydrophobic block by nearly four times ($N_{PB}$ = 170) dilates the dimensions of the hydrophobic cores by about three times (not illustrated here) and shifts the composition window for wormlike micelles (and perhaps vesicles and spherical micelles) to lower values of $w_{PEO}$.

However, the most dramatic structural changes we found were at compositions between the B and C regions. Decreasing the length of the PEO block leads to the formation of Y-junctions in the nominally cylindrical micelles. Even for $w_{PEO}$ = 0.42, which we associate with the C region in Fig. 1, the wormlike micelles contain occasional branches; two have been captured in the cryo-TEM image shown in Fig. 1B. Decreasing $w_{PEO}$ to 0.39 induces striking morphological changes (Fig. 2A). Branched cylindrical loops, branched linear wormlike micelles, and Y-junctions terminated by enlarged spherical caps characterize this representative image. Macroscopically, this solution is opaque (milky) but showed no tendency to

phase separate even after sitting quiescently for several months.

Unlike any of the other specimens examined in this study, dilute mixtures of the $w_{PEO}$ = 0.34 diblock copolymer phase separate macroscopically at room temperature. This process is slow but unmistakable. Several hours to several days after cessation of stirring, an opaque layer develops above a relatively clear majority (water) phase. Increasing the polymer concentration greatly enhances the viscosity, thus slowing macroscopic phase separation; a soft solid gel forms between 22 and 26 wt% block copolymer. We have obtained cryo-TEM images from 1% solutions of this material with mixing protocols that range from gentle stirring to vigorous sonication. In each case, an opaque, low-density phase reemerges after a quiescent period. Figure 2, B and C, illustrates two representative cryo-TEM images of the associated self-assembled structures captured before macroscopic phase separation. This macromolecular surfactant forms an extended three-dimensional network morphology dominated by Y-junctions. Detailed analysis of large pieces of network, like that found in Fig. 2B, is complicated by the density of

**Fig. 1.** Morphology diagram for PB-PEO in water (1 wt%) as a function of molecular size and composition, where $N_{PB}$ and $w_{PEO}$ are the degree of polymerization and weight fraction of the PB and PEO blocks, respectively. Four basic structural motifs—bilayers (B), Y-junctions (Y), cylinders (C), and spheres (S)—have been identified by cryo-TEM, as illustrated in the micrographs, (**A** to **C**). At $N_{PB}$ = 170, decreasing $w_{PEO}$ from the cylindrical condition ($w_{PEO}$ = 0.42) toward that associated with vesicles ($w_{PEO}$ = 0.24) results in an increasing population of Y-junctions. A single-phase dispersion of branched, wormlike micelles at $w_{PEO}$ = 0.39, denoted $C_Y$ (Fig. 2A), is followed by network (N) formation and macroscopic phase separation at $w_{PEO}$ = 0.34 (Fig. 2, B and C). Only the classic structures (B, C, and S) were found at $N_{PB}$ = 46, indicating a fundamental structural transition from classic two-component (surfactant/water) to three-component (surfactant/oil/water) phase behavior above a critical diblock copolymer molecular mass. Speculated (dashed lines) and established (solid lines) morphological boundaries do not reflect precise transition conditions. Open and filled symbols refer to previous (*11*) and current experimental results, respectively. Bars (A to C), 100 nm.

**Scheme 1.**
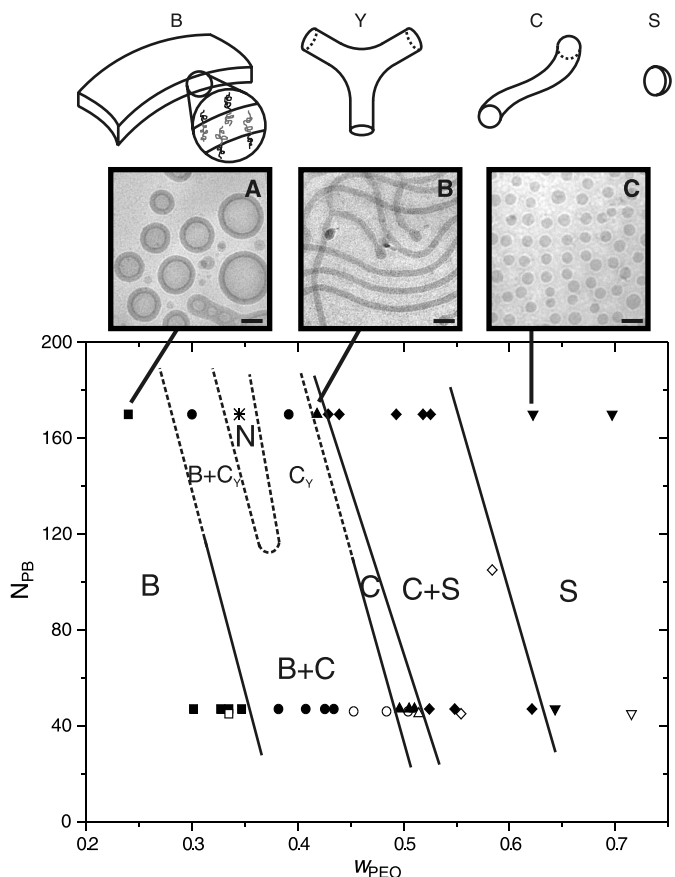
network material spanning the vitrified film, which screens individual features. Nevertheless, the edges of the object captured in Fig. 2B reveal the same general structural elements evident in the smaller fragment presented in Fig. 2C. Decreasing the size of the PEO block (i.e., from $w_{PEO} = 0.42$ to 0.39 to 0.34) increases the population of Y-junctions to the point of network formation and phase separation. We emphasize that a systematic search of $N_{PB} = 46$ diblock copolymer solutions between the B and C states (Fig. 1) failed to uncover such phase behavior (*18*).

Increasing diblock copolymer molecular weight has another notable consequence. The equilibrium solubility in water drops exponentially with the degree of polymerization, resulting in extremely slow exchange dynamics between individual micelles (*19*). Hence, fragmentation of the network phase by stirring or sonication produces a nonergodic dispersion of particles. Until buoyancy forces compact and fuse these particles (smaller particles should survive longer under the action of thermal motion), each is subject to a localized free-energy optimization.

We have exploited this property to produce small, isolated micelles in the 1 wt% $w_{PEO} = 0.34$ aqueous solution by agitation. Representative cryo-TEM images taken from numerous examples are illustrated in Fig. 3. These images tell us much about the self-assembly characteristics of this PB-PEO diblock copolymer. All of these complex micelles (along with the network fragments shown in Fig. 2, B and C) are constructed from only three elements: Y-junctions, spherical end caps, and cylindrical loops. (One of the most distinguishable differences between the $w_{PEO} = 0.34$ and 0.39 dispersions is the nearly complete lack of linear cylinders in the former.) Y-junctions can be found with three spherical caps (Fig. 3A), two caps (Fig. 3, D, E, and H), one cap (Fig. 3, B to D, F to H, J to L, and N), and no caps (Fig. 3, I and M). With just

three exceptions (Fig. 3, F, K, and L), the objects appear to be planar. (To some extent the planar appearance may be driven by confinement within a thin-film geometry.) Y-junctions exhibit a tendency to pair, and to coalesce into periodic arrays. This tendency is evident in micelles containing as few as 2 (Fig. 3, C and D) and as many as 23 (Fig. 3N) junctions.

A striking feature shared by all the micelles presented in Fig. 3 is a high degree of (mirror) symmetry, with the most compelling examples found in panels (A) to (D), (I), and (M). We believe that this symmetry reflects a tendency to balance the internal free-energy through the redistribution of diblock copolymer molecules within the particle after micelle formation by fragmentation (or fusion) (*20*). Because the local movement of PB-PEO molecules is unhindered (the glass transition for the unentangled PB blocks is about –12°C) (*21*), certain rearrangements of the tubular structure are feasible subject to the well-established rules governing microphase separation of monodisperse block copolymers (*22*). Optimization of the particle free-energy will pit the overall surface tension (proportional to the micelle surface area) against chain stretching inside (PB) and outside (PEO) the tubular structure (*23*). The uniformity in core diameters (34 nm on the basis of the cryo-TEM images) found within each micelle and across all micelles is evidence that these rules are operative. Accounting for the recorded shapes and topologies should prove a challenge to self-consistent field theorists working with block copolymers. Even if we ignore "isomerizations" involving topological transitions (i.e., breaking or collapsing loops) (*24*), Y-junctions can be created by sprouting a spherical cap on a cylindrical section with the required polymer drawn from loop sections. The prevalence of spherically capped Y-junctions in Fig. 2, B and C,
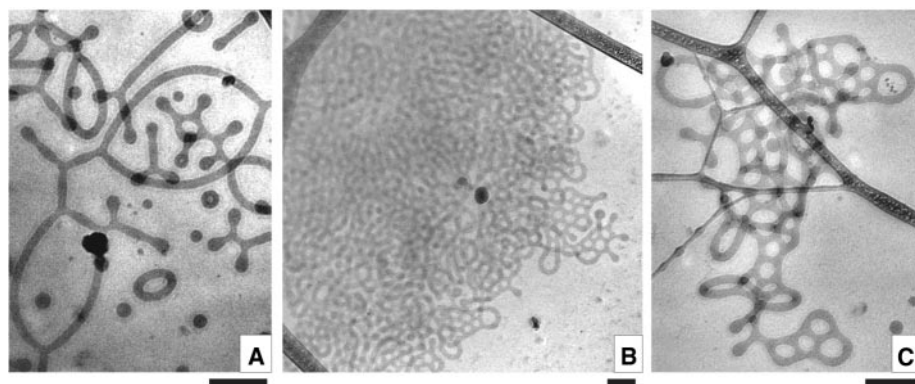


**Fig. 2.** Cryo-TEM images obtained from 1 wt% aqueous solutions of (**A**) $w_{PEO} = 0.39$ and (**B** and **C**) $w_{PEO} = 0.34$ PB-PEO diblock copolymers. The single-phase solution denoted $C_Y$ in Fig. 1 ($w_{PEO} = 0.39$) contains a dispersion of micelles constructed from linear and looped cylindrical segments, Y-junctions, and spherical caps. Macroscopic phase separation at $w_{PEO} = 0.34$ is manifested in large, dense network particles (B) containing a preponderance of loops and Y-junctions. A smaller network fragment (C) provides a more detailed glimpse of the morphology associated with the network phase. Bars (A to C), 200 nm.

**Fig. 3.** (**A** to **N**) Representative cryo-TEM images of network phase fragments obtained after agitating the $w_{PEO} = 0.34$ solution. These micelles are constructed from three structural units: Y-junctions, spherical caps, and cylindrical loops. The high degree of mirror symmetry is speculated to derive from a tendency to balance the local free-energy through transport of diblock copolymer molecules within the reticulated tubular structures.
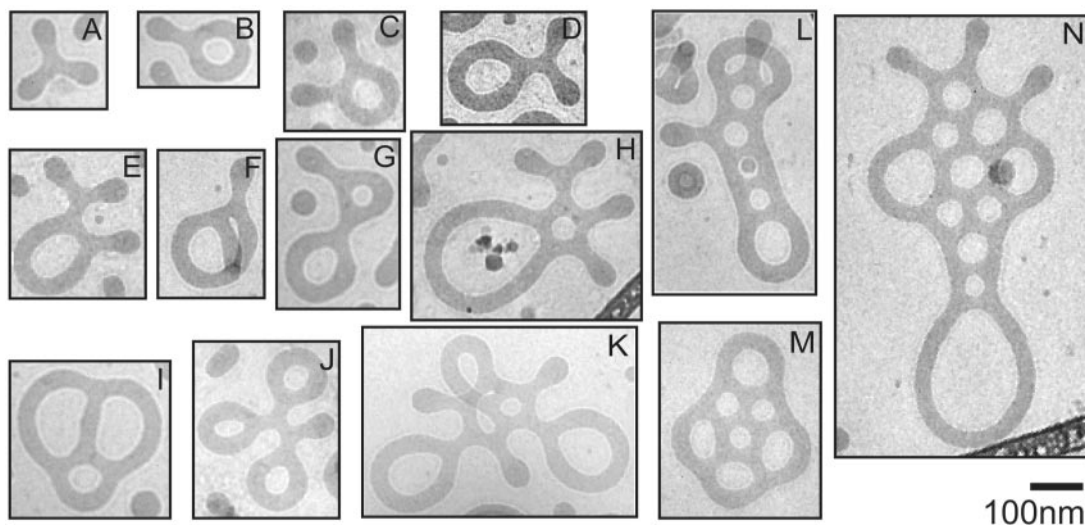
and Fig. 3 suggests that this element is favored over looped cylinders. It is tempting to hypothesize that, given time, particle N (Fig. 3) likely would have added another capped Y-junction by tapping the reservoir of diblock copolymer contained in the large loop, rendering perfect mirror symmetry.

The number of spherical caps relative to closed loops appears to decrease with increasing network particle size (Fig. 2C), leading us to speculate that the equilibrium morphology may be hexagonally ordered perforated sheets constructed solely from Y-junctions. Realizing this morphology on a macroscopic scale may be kinetically impossible, although a perforated vesicle with soccer-ball–style struts seems feasible given the four-, five-, and sixfold coordinated loops found in panels (L), (M), and (N) of Fig. 3, respectively. Small-angle x-ray scattering patterns taken from the dense network phase (e.g., the gelled 26 wt% specimen) indicate that the local domain curvature remains nearly cylindrical in this limit (Fig. 4).

Branching in cylindrical dispersions is not a new concept (25, 26). Tlusty and Safran (27) hypothesized several years ago that under appropriate conditions Y-junctions would appear in cylinder-forming three-component (surfactant/oil/water) microemulsions, leading to network formation and phase separation (28, 29). Recently Bernheim-Groswasser et al. (15, 30) presented elegant cryo-TEM images obtained with a low molecular weight nonionic surfactant ($C_{12}E_5$) mixed with water and n-octane that demonstrates such branching. Our results (Figs. 2 and 3) are strikingly similar to the theoretic predictions in several ways. Tlusty et al. (13) predict the same sequence of topological transitions that we report in Fig. 1 for $N_{PB} = 170$. This comparison suggests that the quantity $w_{PEO}$ for the two-component diblock copolymer/water system is analogous to $c_oR$ in the three-component surfactant/oil/water system, where $c_o$

is the spontaneous curvature and $R$ the domain radius. There appears to be a threshold molecular weight above which block copolymer surfactants can exhibit microemulsion phase behavior in water without the addition of a third component. We speculate that the conformational freedom associated with high molecular weight PB blocks facilitates domain packing in complex geometries like the network junction without the addition of hydrocarbon solvent. The short and relatively inflexible hydrocarbon portions of conventional surfactants (e.g., a $C_{12}$ unit) require added oil to ensure a constant domain density under comparable conditions.

Even certain detailed morphological predictions appear to be supported by our results. For example, the bulbous spherical end caps found in Figs. 2 and 3 closely resemble those anticipated by Tlusty and Safran (31), and the notion that the distance between junctions is comparable with their size as $c_o \rightarrow 0$ is illustrated dramatically by the junction coalescence evident in the cryo-TEM images in Figs. 2 and 3.

These findings offer insights into the origins of morphological complexity in block copolymer/water mixtures (6–8) along with new opportunities for designing soft materials with enhanced properties. Reduction in the number of components required to create junctions and networks is of great practical value. We anticipate that the reported morphologies will be weakly dependent on temperature, in contrast to nonionic surfactant-based systems where $c_o$ is highly temperature dependent, resulting in narrow microemulsion windows (13). In addition, macromolecular surfactancy should be universal, with phase behavior described by molecular composition and the relative interfacial interaction energy. Finally, the dimensional control demonstrated here can be amplified through manipulation of the core-block physical properties—for example, glassy, semicrystalline,

cross-linked–rubbery, and liquid-like—a degree of materials design flexibility not available with low molecular weight amphiphiles.

**References and Notes**
1. W. M. Gelbart, A. Ben-Shaul, *J. Phys. Chem.* **100**, 13169 (1996).
2. D. F. Evans, H. Wennerstrom, *The Colloidal Domain: Where Physics, Chemistry, Biology, and Technology Meet* (VCH, New York, ed. 2, 1998).
3. P. Alexandridis, B. Lindman, Eds., *Amphiphilic Block Copolymers: Self-Assembly and Applications* (Elsevier, New York, 2000).
4. Y.-Y. Won, H. T. Davis, F. S. Bates, *Science* **283**, 960 (1999).
5. B. M. Discher et al., *Science* **284**, 1143 (1999).
6. L. Zhang, A. Eisenberg, *Science* **268**, 1728 (1995).
7. K. Yu, L. Zhang, A. Eisenberg, *Langmuir* **12**, 5980 (1996).
8. S. Burke, A. Eisenberg, *High Perform. Polym.* **12**, 535 (2000).
9. Y.-Y. Won, H. T. Davis, F. S. Bates, M. Agamalian, G. D. Wignall, *J. Phys. Chem. B* **104**, 9054 (2000).
10. K. Krishnan, K. Almdal, W. R. Burghardt, T. P. Lodge, F. S. Bates, *Phys. Rev. Lett.* **87**, 098301/1 (2001).
11. Y.-Y. Won, A. K. Brannan, H. T. Davis, F. S. Bates, *J. Phys. Chem. B* **106**, 3354 (2002).
12. J. Israelachvili, *Intermolecular and Surface Forces* (Academic Press, San Diego, CA, ed. 2, 1992).
13. T. Tlusty, S. A. Safran, R. Strey, *Phys. Rev. Lett.* **84**, 1244 (2000).
14. J. T. Kindt, *J. Phys. Chem. B* **106**, 8223 (2002).
15. A. Bernheim-Groswasser, T. Tlusty, S. A. Safran, Y. Talmon, *Langmuir* **15**, 5448 (1999).
16. S. Y. Kwon, M. W. Kim, *Phys. Rev. Lett.* **89**, 258302 (2002).
17. M. A. Hillmyer, F. S. Bates, *Macromolecules* **29**, 6994 (1996).
18. Cryo-TEM experiments reported by Won et al. (11) revealed unusual polymorphism with block copolymers with $N_{PB}$ and $N_{PEE} = 46$, where PEE refers to poly(ethylethylene). However, almost all branching, including starfish-like structures, was generated by PEO.
19. Y. Y. Won, H. T. Davis, F. S. Bates, *Macromolecules* **36**, 953 (2003).
20. The tendency toward mirror symmetry and the associated explanation based on local free-energy equilibration remains valid in the limit of thin-film confinement.
21. J. D. Ferry, *Viscoelastic Properties of Polymers* (Wiley, New York, ed. 3, 1980).
22. F. S. Bates, G. H. Fredrickson, *Phys. Today* **52**, 32 (1999).
23. The fluid character of the diblock copolymers also provides a mechanism for relaxing stress within curved loop sections. Excess diblock copolymer can move to the outer portion of a looped cylinder, thereby accommodating the extra surface area without unfavorable chain stretching or compression.
24. Loops can be eliminated by shrinkage to the point of fusion or cleavage of a cylindrical section or Y-junction in a closed loop. Both mechanisms are inconsistent with the tendency to increase the number of Y-junctions and the absence of linear (as opposed to looping) cylindrical sections in the quiescent particles (Fig. 2, B and C, and Fig. 3). The most likely transition mode for long cylindrical loops is to produce a spherical cap, which may fuse with cylindrical segments (looped or linear), similar to the theoretical mechanism proposed by Tlusty et al. (13). This sequence would account for the growth of a macroscopic three-dimensional network during particle consolidation under the influence of gravity. Agitation can disrupt this fragile network, breaking off pieces that contain specific topologies dictated by the number of closed loops.
25. G. Porte, R. Gomati, O. El Haitamy, J. Appell, J. Marignan, *J. Phys. Chem.* **90**, 5746 (1986).
26. A. Khatory, F. Lequeux, F. Kern, S. J. Candau, *Langmuir* **9**, 1456 (1993).
27. T. Tlusty, S. A. Safran, *Science* **290**, 1328 (2000).

**Fig. 4.** Small-angle x-ray scattering pattern obtained from a 26 wt% aqueous solution of the $w_{PEO} = 0.34$ PB-PEO diblock copolymer. The solid curve was obtained with the form factor (9) for an ensemble of randomly arranged, noninteracting, infinitely long, and radially nearly monodisperse ($R = 19 \pm 1$ nm) solid cylinders. Close agreement between the broad periodic intensity oscillations in the calculated and experimental scattering patterns, and the mean core dimension extracted from the cryo-TEM images in Fig. 3 ($R = 17$ nm), corroborate a nearly solid cylindrical geometry for the network morphology. Better agreement between the calculated and experimental results requires a theoretical form factor for the Y-junctions.
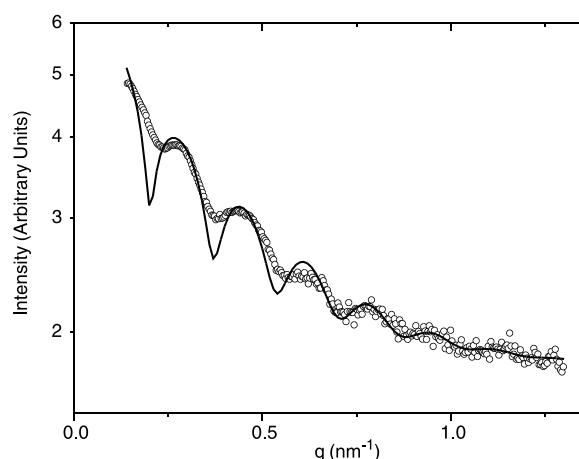
28. T. J. Drye, M. E. Cates, *J. Chem. Phys.* **96**, 1367 (1992).
29. P. Panizza, G. Cristobal, J. Curtly, *J. Phys. Cond. Matter* **10**, 11659 (1998).
30. A. Bernheim-Groswasser, E. Wachtel, Y. Talmon, *Langmuir* **16**, 4131 (2000).
31. T. Tlusty, S. A. Safran, *J. Phys. Cond. Matter* **12**, A253 (2000).
32. This research program was supported by the NSF-sponsored Materials Science and Engineering Center (MRSEC) at the University of Minnesota and by

# Multifunctional Alloys Obtained via a Dislocation-Free Plastic Deformation Mechanism

Takashi Saito,[1]* Tadahiko Furuta,[1] Jung-Hwan Hwang,[1] Shigeru Kuramoto,[1] Kazuaki Nishino,[1] Nobuaki Suzuki,[1] Rong Chen,[1] Akira Yamada,[1] Kazuhiko Ito,[1] Yoshiki Seno,[1] Takamasa Nonaka,[1] Hideaki Ikehata,[1] Naoyuki Nagasako,[1] Chihiro Iwamoto,[2] Yuuichi Ikuhara,[2] Taketo Sakuma[3]

We describe a group of alloys that exhibit "super" properties, such as ultralow elastic modulus, ultrahigh strength, super elasticity, and super plasticity, at room temperature and that show Elinvar and Invar behavior. These "super" properties are attributable to a dislocation-free plastic deformation mechanism. In cold-worked alloys, this mechanism forms elastic strain fields of hierarchical structure that range in size from the nanometer scale to several tens of micrometers. The resultant elastic strain energy leads to a number of enhanced material properties.

Mechanical properties, such as strength, of metallic materials are strongly affected by metallurgical processes such as heat treatment and plastic working, which bring modifications in the microstructure. On the other hand, these processes have no substantial effect on physical properties such as elastic modulus and thermal expansion. The reason for this is that the changes that can be affected by plastic working and heat treatment do not extend to interatomic bonds or electronic states.

We present a group of alloys that exhibit multiple "super" properties and drastic changes in physical properties after plastic working at room temperature. These alloys simultaneously offer super elasticity, super strength, super cold-workability, and Invar and Elinvar properties. The alloys consist of Group IVa and Va elements and oxygen and share the following three electronic magic numbers: (i) a compositional average valence electron number [electron/atom (e/a) ratio] of about 4.24; (ii) a bond order (Bo value) of about 2.87 based on the DV-Xα cluster method, which represents the bonding strength (*1–3*); and (iii) a "d" electron-orbital energy level (Md value) of about 2.45 eV, representing electronegativity. The properties

emerge only when all three of these magic numbers are satisfied simultaneously. Various alloy composition combinations meet these criteria, such as Ti-12Ta-9Nb-3V-6Zr-O and Ti-23Nb-0.7Ta-2Zr-O [mole percent (mol %)], wherein each alloy has a simple body-centered cubic (bcc) crystal structure. In order to exhibit these properties, each alloy system requires substantial cold working and the presence of a certain amount of oxygen, restricted to an oxygen concentration of 0.7 to 3.0 mol %.

Typical properties of the alloys are shown in Fig. 1 for samples before and after cold swaging with 90% reduction in area (*4*). Tensile stress-strain curves shown in Fig. 1A indicate that cold working substantially decreases the elastic modulus and increases the yield strength

and confirm nonlinearity in the elastic range, with the gradient of each curve decreasing continuously to about 1/3 its original value near the elastic limit. As a result of this decrease in elastic modulus and nonlinearity, elastic deformability after cold working reaches 2.5%, which is at least double the value before cold working. Generally, large elastic deformations that occur in so-called "super-elastic alloys" are known to be reversible martensitic transformations resulting from deformation, dubbed "pseudo-elastic deformation" (*5, 6*). Conversely, the large elastic deformation in the alloy studied is an intrinsically different "true-elastic deformation," which is not accompanied by phase transformation. The elastic deformability of the cold-worked material has been found to increase with decreasing temperature, exceeding 4% at 77 K. The strength of the alloy increases with decreasing temperature, as in normal metals, reaching 1800 MPa at 77 K. Conversely, the elastic modulus of non-cold-worked samples increases with decreasing temperature, in the same manner as for normal metals, but, as shown in Fig. 1B, the elastic modulus of the cold-worked alloy remains about constant between 77 and 500 K. Elinvar alloys (*7*), which maintain a constant elastic modulus over a limited temperature range, have already been known. However, none of them has been known to maintain a constant elastic modulus over such a wide temperature range. Figure 1C shows the temperature dependence of linear expansion. In an annealed state, the alloy exhibits almost linear thermal expansion behavior similar to that of a normal metal and continues to expand with increasing temperature. Its linear expansion coefficient is about $8 \times 10^{-6}$ K$^{-1}$. For the cold-worked alloy, the linear expansion coefficient does not exceed
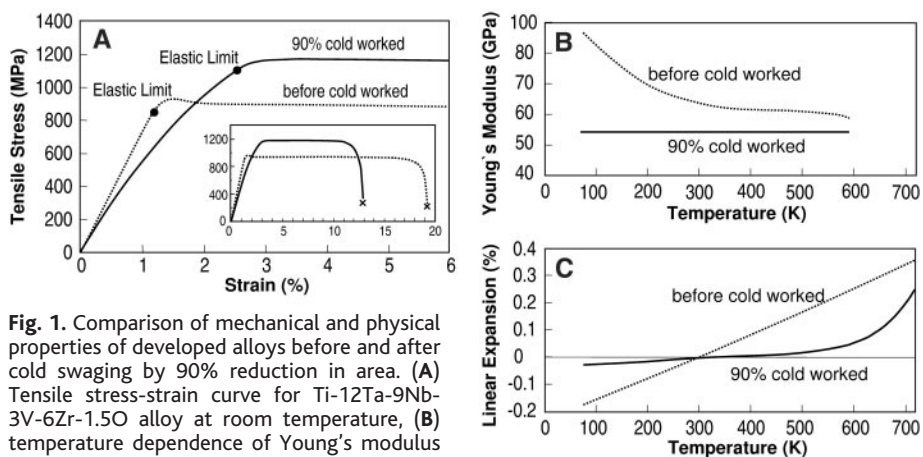


**Fig. 1.** Comparison of mechanical and physical properties of developed alloys before and after cold swaging by 90% reduction in area. (**A**) Tensile stress-strain curve for Ti-12Ta-9Nb-3V-6Zr-1.5O alloy at room temperature, (**B**) temperature dependence of Young's modulus near zero stress in Ti-23Nb-0.7Ta-2Zr-1.2O alloy, and (**C**) temperature dependence of linear expansion in Ti-23Nb-0.7Ta-2Zr-1.2O alloy.

[1]Toyota Central Research and Development Laboratories, Incorporated, Nagakute Aichi, 480-1192 Japan. [2]Institute of Engineering Innovation, University of Tokyo, Hongo, Bunkyo-ku, Tokyo, 113-8656 Japan. [3]Graduate School of Frontier Sciences, University of Tokyo, Hongo, Bunkyo-ku, Tokyo, 113-0033 Japan.

*To whom correspondence should be addressed. E-mail: saito@mosk.tytlabs.co.jp